THE JOURNAL OF PHYSICAL CHEMISTRY B LETTERS

2009, *113,* 12623–12627
Published on Web 08/31/2009

Evaluation on Pore Structures of Organosilicate Thin Films by Grazing Incidence Small-Angle X-ray Scattering

Hong-Ji Chen,*,† Sheng-Ying Li,† Xiao-Jun Liu,† Rui-Peng Li,‡ Detlef-M. Smilgies,‡ Zhong-Hua Wu,§ and Zhihong Li§

Department of Material Science & Engineering, Jinan University, Guangzhou 510632, P. R. China, Materials Science and Engineering, Cornell University, Ithaca, New York 14853, Cornell High Energy Synchrotron Source, Cornell University, Ithaca, New York 14853, and Corning Inc., SP-FR-6, Corning, New York 14830, and Beijing Synchrotron Radiation Facility, Institute of High Energy Physics, Chinese Academy of Sciences, Beijing 100039, P. R. China

Received: June 10, 2009; Revised Manuscript Received: August 23, 2009

Nanoporous thin films fabricated by both a core−shell-shaped organic−inorganic hybrid sphere (octa(2,4-dinitrophenyl)silsesquioxane, ODNPSQ) and a four-leg-numbered surfactant (polyoxyethylene sorbitan monolaurate, Tween-20) for porogens in a higher molecular weight precursor (polyphenylsilsesquioxane, PPSQ) were characterized, respectively, by grazing incidence small-angle X-ray scattering (GISAXS), and the measured 2D GISAXS profiles were analyzed quantitatively by using a GISAXS formula based on the distorted wave Born approximation (DWBA). The fitted 2D GISAXS data show that the PPSQ porous thin films imprinted with ODNPSQ porogen exhibit sphere-shaped closed pores with the average pore size within a range of 1.18−3.12 nm and pore size distribution widths about 3.0 nm when the porogen loadings increase from 10 to 40 wt % and those imprinted with Tween-20 porogen give out an average pore size of 1.07−1.29 nm and pore size distribution widths about 2.0 nm with the porogen loading varying from 5 to 30 wt %. The nanoporous dielectric thin films imprinted with ODNPSQ porogen show a reducing to the molecular aggregation of porogens and significant antiphase separation behavior in the cross-linked matrix.

Silica-based porous thin film materials have received considerable attention due to their structural and pattern diversity,[1,2] physicochemical properties, and potential applications, including catalyst supporting materials,[3] sensors,[4−6] integrated circuits,[7−11] optical components,[12] and biosubstrates.[13] Challenges come from different fabrication technologies of thin films[14] and controlling methods of pore structural parameters (pore shape, pore size, pore distribution, and so on) as well. In order to obtain fine defined nanopores in organosilicate matrixes, numerous effective approaches, such as template pores by self-assembly of surfactants,[15−18] ionic liquids,[19] organic copolymer,[20] supercritical fluids[21] with silsesquioxanes, vapor phase synthesis,[22] thermo-sacrificial dendritic organic pore generators (porogens) in silsesquioxane precursors,[23−27] and inorganic−organic hybrid copolymers,[9,11] have been designed and studied in recent years. The above reported porous materials prepared from the silsesquioxane precursor, mostly polymethylsilsesquioxane (PMSSQ), with organic pore generator or porogen obey the principle of microphase separation,[28−30] namely, let the phase-separated organic compounds first form domains of nanometers within inhomogeneous systems and then decompose them by thermal curing or UV-aided thermal curing, leaving "footprints" in the cross-linked matrix. In order to explore physicochemical properties of silica-based porous thin film materials, the evaluation of pore structural parameters is helpful and significant. If the film materials contain open-pore or channel structures, they are able to be developed for potential applications in gas sorption, gas separation, and catalyst supporters. However, such porous materials generally can result in unfavorable mechanical properties (such as poor modulus, hardness, fracture toughness, adhesion, and low breakdown voltage) as well, which are critical parameters for porous materials to achieve successful fabrication of integrated circuits. Thus, the thin film materials with closed pores are more suitable for application in ultralow dielectric constant (ULK) materials. However, nanoscaled pore structural characteristics of thin film materials were not investigated extensively; the accurate determination of nanoscaled pore structural parameters for them remains a challenge. Grazing incidence small-angle X-ray scattering (GISAXS) is an effective tool for analysis of nanoporous thin film materials, especially in the cases that the pore size of materials is beyond subnanometer and traditional analysis instruments and methods (such as scanning electron microscopy (SEM), transmission electron microscopy (TEM), and atomic force microscopy (AFM)) are unapproachable.[2,31,32]

For the interests in researching nanoporous thin films and their application in integrated circuits (ULK materials), we reported the synthesis of precursor polyphenylsilsesquioxane (PPSQ) and porogen octa(2,4-dinitrophenyl)silsesquioxane (ODNPSQ) and the fabrication method of porous thin films imprinted by core−shell-shaped organic−inorganic hybrid

* Corresponding author. E-mail: thjchen@jnu.edu.cn. Phone: 86-020-85221362. Fax: 86-020-85223271.
† Jinan University.
‡ Cornell University and Corning Inc.
§ Chinese Academy of Sciences.

10.1021/jp905457b CCC: $40.75

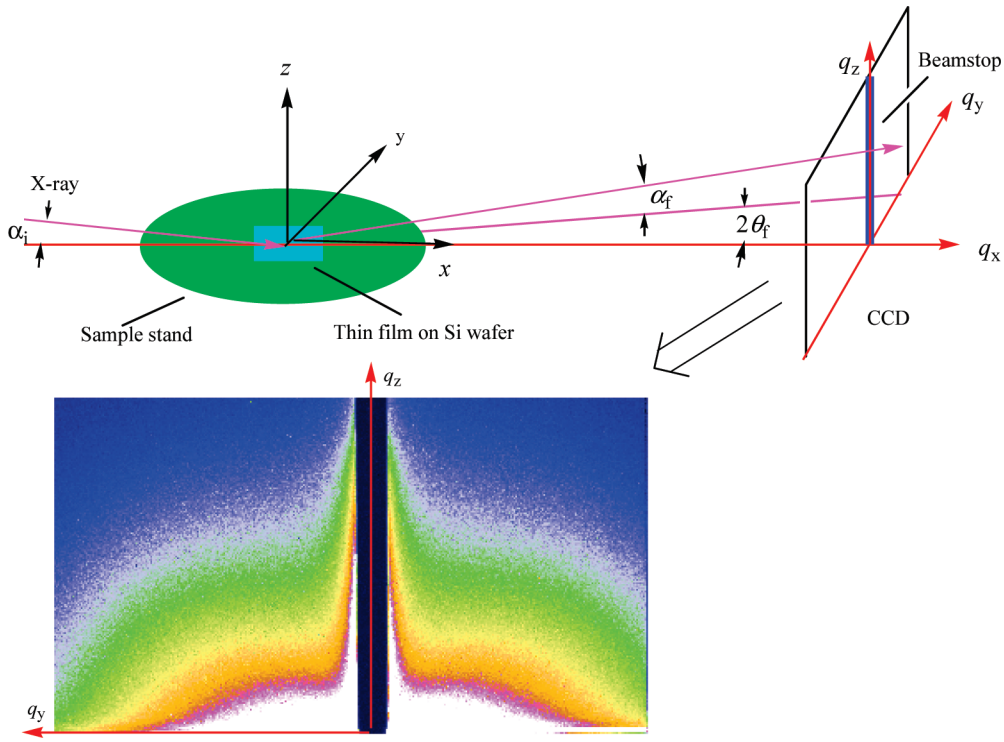

Figure 1. GISAXS profile of a nanoporous PPSQ thin film deposited onto a silicon substrate. (top) Geometry of GISAXS with a 2D CCD detector, where α_i and α_f are the incident angle of the X-ray beam and the exit angle with respect to the thin film surface and $2\theta_f$ is the scattering angle with respect to the plane of incidence. (bottom) One typical 2D GISAXS pattern obtained at $\alpha_i = 0.175°$ for an ~500 nm thick nanoporous thin film imprinted with 30 wt % porogen.

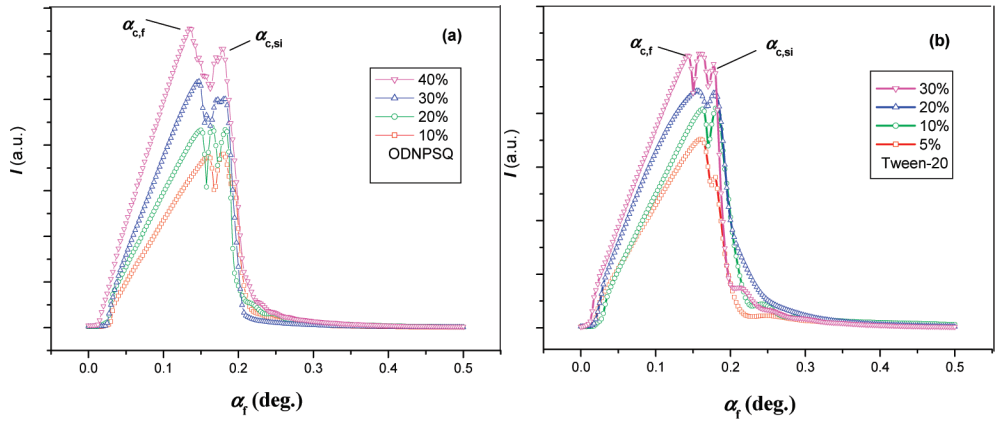

Figure 2. Out-of-plane GISAXS profiles obtained at $2\theta_f = 0.156°$ from 2D GISAXS patterns of PPSQ thin films imprinted by ODNPSQ (a) and Tween-20 (b): $\alpha_{c,f}$ and $\alpha_{c,si}$ are the critical angles of the thin film and the silicon substrate, respectively.

sphere ODNPSQ and four-leg-shaped surfactant polyoxyethylene sorbitan monolaurate (Tween-20) in the PPSQ matrix, respectively, in previous work.[27] Here, we report the evaluation of their pore structural parameters using the grazing incidence small-angle X-ray scattering method[33] (Figure 1).

A group of out-of-plane GISAXS profiles obtained at $2\theta_f = 0.156°$ from the porous PPSQ thin films imprinted by the ODNPSQ and Tween-20 porogens is shown in Figure 2. All thin films show very low scattering strength at small $2\theta_f$ angle. By raising the $2\theta_f$ angle, the scattering strength increases to the first high value at $\alpha_{c,f}$ and then to the maximum at $\alpha_{c,si}$. After that, the scattering strength of the thin films decreases quickly, showing an oscillation profile. The $\alpha_{c,f}$ values for all of the thin films imprinted by the ODNPSQ are located at 0.143−0.163° with the increasing of the porogen loadings from 10 to 40 wt % (ODNPSQ-10 to ODNPSQ-40), and the $\alpha_{c,si}$ values for the thin films are essentially independent of the porogen loadings. Seminar to ODNPSQ, the $\alpha_{c,f}$ values for all of the thin films imprinted by Tween-20 are located at about 0.135−0.16° with the porogen loadings increasing from 5 to 30 wt % (Tween-20-5 to Tween-20-30), and the $\alpha_{c,si}$ values for the thin films are independent of the porogen loadings as well.

All 2D GISAXS patterns were measured at incidence angles in the range 0.15−0.30°. When the incident angle of the X-ray beam (α_i) is less than 0.15° (the critical angle of the thin film, $\alpha_{c,f}$) or larger than 0.25° (the critical angle of the silicon substrate, $\alpha_{c,si}$), the scattering intensities of GISAXS patterns are weak. However, when α_i is located between $\alpha_{c,f}$ and $\alpha_{c,si}$, the intensities of GISAXS patterns are relatively strong and almost independent of the incident angle of the X-ray beam but depend on the porosities, i.e., the initial porogen loading. The 2D GISAXS patterns give out bright scattering features without preferential orientations along the $2\theta_f$ axis direction, which is due to a type of standing wave phenomenon from total

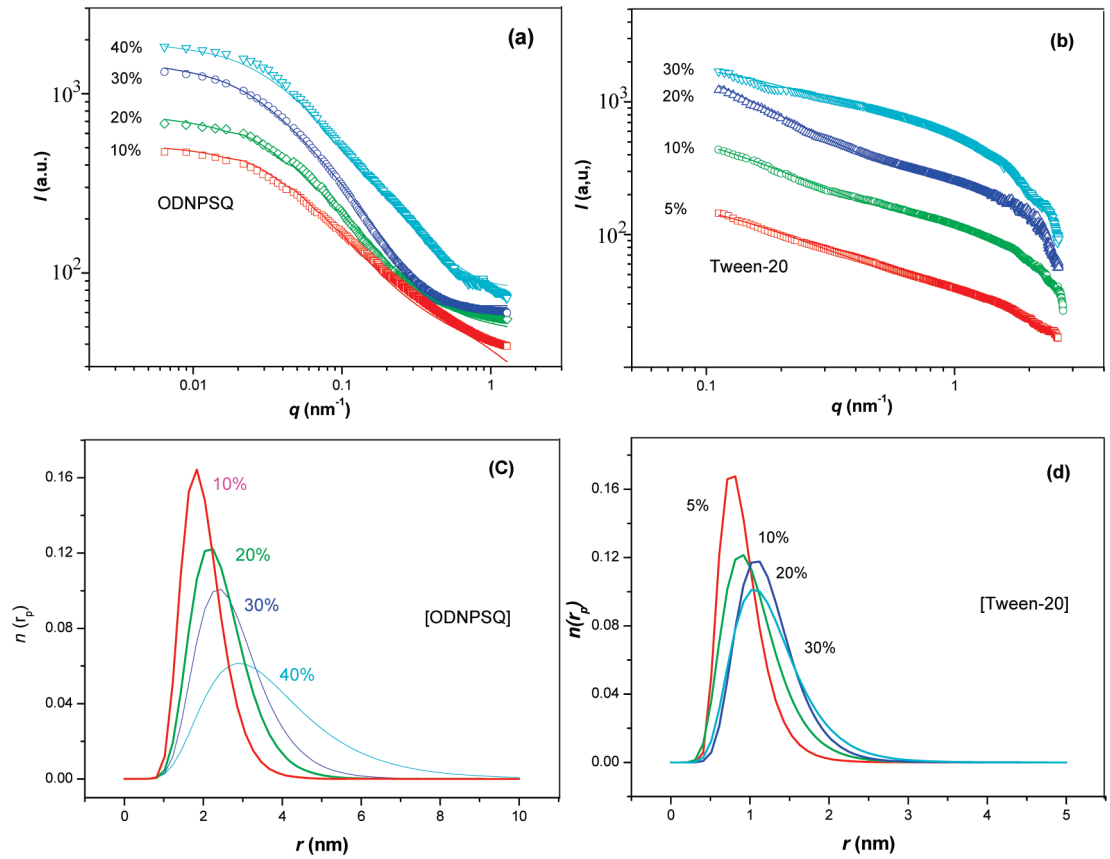

Figure 3. GISAXS profiles along the q_y direction at an exit angle of 0.18° from the 2D GISAXS patterns measured for PPSQ thin films imprinted with ODNPSQ (a) and Tween-20 porogen (b). Pore size and distribution determined at an exit angle of 0.175° obtained from the 2D GISAXS patterns measured for nanoporous PPSQ thin films imprinted with ODNPSQ (c) and Tween-20 (d): Here, the percentages indicate the initial porogen loadings, the symbols are the measured data, and the solid lines are the fitted data with a GISAXS formula derived from the distorted wave Born approximation; $n(r_p)$ is the log-normal size distribution and volume of pore with radius.

reflection at the interface between the film and the substrate and indicates all pores are randomly distributed in the in-plane and out-of-plane of the porous thin films. By fixing or changing out-of-plane exit angles (α_f) between $\alpha_{c,f}$ and $\alpha_{c,si}$, 1D GISAXS profiles were extracted along the q_y direction, showing similar shapes but different intensities. All 1D GISAXS profiles were extracted from the measured 2D GISAXS patterns along the q_y direction using the FIT2D software, and they are plotted in Figure 3a and b.

GISAXS formulas based on Lazzari's software program "IsGISAXS"[34−36] were used to analyze the data quantitatively. The form factor within the distorted wave Born approximation (DWBA) is based on a framework of particles encapsulated in an overlayer. The scattering cross section for a buried particle was derived by Rauscher with $n_i = 1$ for the void. The size-spacing correlation approximation model and s−s polarization of the incident and scattered waves were used.[37,38] To analyze the extracted in-plane GISAXS profiles by using the IsGISAXS program, we considered all possible scattering models for the scattering intensity from pores in the thin films and found that the full sphere model with a log-normal size distribution is the most suitable for the measured GISAXS profiles. The wave amplitudes in the thin films were calculated by using the Parratt formula and the scattering strengths by the Pedersen formula with the spherical particle and a log-normal size distribution.[39,40]

The GISAXS scattering profiles of PPSQ thin films imprinted with ODNPSQ porogens were fitted well by the GISAXS formulas in the program, indicating that the pores in the porous thin films are spherical and have a sharp interface with the PPSQ matrix. From the above analysis, the resulting sizes and distributions of the pores were determined and summarized in Figure 3c and Table 1. It was also found that the PPSQ thin film imprinted with ODNPSQ-10 has an average gyration radius of pores of 0.83 nm, which is reasonable for the corresponding radius of gyration of the pore (0.80 nm) determined by using small-angle X-ray scattering (SAXS) in toluene. The average radius of the pores imprinted with ODNPSQ-10 is 1.18 nm, and the corresponding pore distribution width is about 3.0 nm. With an increase of loading percent, the average radius of the pores and the average gyration radius of pores for the PPSQ thin films from ODNPSQ-10 to ODNPSQ-40 vary in the ranges 1.18−3.12 and 0.83−2.02 nm, respectively. The results of PPSQ thin film imprinted with ODNPSQ porogen told us that the pore sizes enlarge with increasing porogen loading but no large pores appear in the matrix until a high porogen loading of 40 wt %, which is similar to the results of porous PMSSQ thin films imprinted with high-leg-numbered (32 and 64) thermally labile porogens.[23] We attribute the small pore size and narrow pore distributions for the PPSQ thin films from ODNPSQ to the following two principal factors: (1) The star-shaped and 16-leg-numbered ODNPSQ molecule contains a cage-like molecular structure and smaller average gyration radius of pores (0.83 nm). The Si−O−Si covalent bond angles in the cubic Si_8O_{12} core of the porogen molecule are more bent/compressed and can store more bond energy than those of porogens with flexible molecular structure;[24−26,30] they are able to escape out more potential energy at decomposition temperature to create a bigger pore size than its average gyration radius of pores in the cross-

TABLE 1: Pore Structures and Properties of PPSQ Thin Films Imprinted with Both ODNPSQ and Tween-20 Porogens

	porogen loading		pore size and electron density				porosity and dielectric constant				
thin film samples	porogen	(wt %)	r_1[a] (nm)	r_2[b] (nm)	R_g[c] (nm)	ρ_e (nm^{-3})	n_{RI}[d]	P_1[e] (%)	ε_∞[f]	P_2[g] (%)	ε[h]
ODNPSQ-10	ODNPSQ	10	1.18	1.84	0.83	366	1.59	8.6	2.52	8.3	2.81
ODNPSQ-20	ODNPSQ	20	1.93	2.25	1.76	322	1.53	16.3	2.34	19.3	2.49
ODNPSQ-30	ODNPSQ	30	2.45	2.45	2.20	311	1.42	27.3	2.10	22.1	2.25
ODNPSQ-40	ODNPSQ	40	3.12	2.86	1.94	261	1.39	35.8	1.93	35.0	2.11
Tween-20−5	Tween-20	5	0.82	1.07	0.95	366				8.3	2.89
Tween-20-10	Tween-20	10	0.92	1.15	1.00	378	1.56	12.4	2.43	5.3	2.84
Tween-20-20	Tween-20	20	1.12	1.18	0.82	343	1.51	19.0	2.28	14.0	2.52
Tween-20-30	Tween-20	30	1.02	1.29	1.30	290	1.42	31.5	2.01	27.3	2.30

[a] Porous average radius corresponding to the maximum of the log-normal pore size distribution. [b] Average radius estimated from the radius r and the number distribution of pores. [c] Average radius of gyration estimated from the radius r and the volume distribution of pores. [d] Refractive index measured at 632.6 nm using spectroscopic ellipsometry. The data are from ref 27. [e] Porosity estimated from the measured refractive index using the Lorentz−Lorenz equation. The data are from ref 27. [f] Dielectric constants measured at 632.6 nm using spectroscopic ellipsometry. The data are from ref 27. [g] Porosity estimated from the electron density. [h] Dielectric constants measured at 1 MHz using an impedance analyzer.

linked matrix. (2) The core−shell-shaped organic−inorganic hybrid spheres have a lipophilic shell constructed from the outer layer eight dinitrophenyl groups; the adjacent nitro groups of the porogen molecules do not form hydrogen bonds. Molecular aggregates come from intermolecular $\pi-\pi$ interactions of the porogen molecules. Adjacent dinitrophenyl groups of the porogen molecules can be linked together in a "face-to-face" way through $\pi-\pi$ interactions and then form molecular aggregates; such molecular aggregates are weaker than those from general hydrogen bonds, so that it is not possible to form domains of nanometers in the PPSQ/ODNPSQ system and create a large pore size through phase separation in the matrix. We can control the pore size within 3 nm for the porous PPSQ thin films imprinted with ODNPSQ even if the porogen loading is high up to 40%.

In contrast, the four-leg-numbered surfactant Tween-20 contains hydroxyl and carboxyl groups, which are able to form O−H···O hydrogen bonds among the porogen molecules, resulting in molecular aggregation. Although the GISAXS scattering profiles of PPSQ thin film imprinted with 5−30 wt % Tween-20 porogen can be fitted by the GISAXS formulas with the full sphere model, those of the films fabricated by the porogen loading beyond 30 wt % could not be fitted through the program with different models. The molecular size of Tween-20 porogen was determined in methyl isobutyl ketone (MIBK) using SAXS with a measured average radius of gyration of 0.90 nm. It was found from the GISAXS analysis results of PPSQ thin films imprinted with 5−30 wt % Tween-20 porogen that the values of the average radius of pores and average gyration radius of pores for the PPSQ thin films from Tween-20-5 to Tween-20-30 are within a range of 1.07−1.29 and 0.95−1.30 nm, respectively (Figure 3d and Table 1). Before phase separation, the pore sizes of PPSQ thin films imprinted with 5−30 wt % Tween-20 porogen are smaller than those of PPSQ thin films imprinted with ODNPSQ porogen. When the Tween-20 porogen loading is higher than 30 wt %, strong phase separation happened in the system, resulting in large and linked pores with a size of 40−80 nm in the matrix.[27] This is similar to the behavior of phase separation for most low-leg-numbered (<8) thermally labile porogens in the PMSSQ matrix[24] but with a smaller pore size than that (400 nm) for the porous thin films generated from the four-leg-shaped porogen in the PMSSQ matrix.[25]

A good miscibility/compatibility between template molecules and silsesquioxane precursors before and after curing is important for control over the final pore structural parameters. A possible phase separation behavior was proposed by Miller and co-workers.[19] Molecular aggregations of template molecules are first ignited through intermolecular forces (hydrogen bonds, static attractive, $\pi-\pi$ interactions), then the sizes and shapes of molecular aggregations are grown to domains, and then these domains are finally separated in the inhomogeneous systems at a thermodynamic unstable state. However, the sizes and shapes of these domains coming from self-assembly of molecules are uncontrollable. It was found from the results that high-leg-numbered thermally labile porogen (ODNPSQ) can form small scale molecular aggregates only, but low-leg-numbered thermally labile porogen (Tween-20) can form both small and large scale molecular aggregates depending on its concentration. In small scale molecular aggregates, the size and size distribution of pores depend on the porogen loading. Large scale molecular aggregates generate strong phase separation behavior and produce big open pores or channels in the matrixes after curing. Moreover, suitable solvents are helpful for offering good miscibility/compatibility between template molecules and silsesquioxane precursors. We used one mixture solution of xylene, MIBK, and tetrahydrofuran (THF) at a ratio of about 1:1:1 (v/v/v) for the ODNPSQ/PPSQ system and another one of toluene and MIBK at a ratio of 3:1 (v/v) in the Tween-20/PPSQ system, respectively. The electron densities of thin films were estimated from the GISAXS profiles, and then, the corresponding porosities were calculated from the resulting data (Table 1), showing the values of porosities are in the range 8.3−35.0% for ODNPSQ porogen and 8.3−27.3% for Tween-20 porogen, which are similar to the results from the porous PPSQ thin films investigated and estimated by the Lorentz−Lorenz relationship. The resulting electric measurement data show that porous PPSQ thin films from ODNPSQ porogen exhibit lower dielectric constants than those of corresponding porous PPSQ thin films from Tween-20 porogen. The values of dielectric constant (ε_∞) at high frequency (633 nm or 4.47×10^{14} Hz) are in the range 2.66−1.93 for porous PPSQ thin films from ODNPSQ and 2.62−2.02 for Tween-20 porogen, which show a reduction from the PPSQ matrix ($\varepsilon_\infty = 2.83$). Their dielectric constants (ε) at low frequency (1 MHz) are in the range 2.81−2.11 and 2.89−2.30, respectively. However, all ε_∞ values of PPSQ porous thin films are higher than those of corresponding PMSSQ porous thin films.[28−30] According to the Debye equation and a recent explanation about the dielectric permittivity of silicates,[41,42] the high-frequency dielectric constant ε_∞ is determined mainly by electric polarization permittivity and the low-frequency dielectric constant ε by all polarization permittivities (including electronic,

ionic, orientational, and so on). From the chemical structural analysis, phenyl substituted silicate is easier to produce distortion of electron clouds in its atoms than that of methyl substituted silicate so that it should exhibit a higher electronic polarization permittivity than that of methyl substituted silicate at high frequency.

In summary, we discussed a feasible method for decreasing molecular aggregations and large scale phase separations existed in the organosilicate dielectrics through improvement of the miscibility and compatibility between the precursors and porogens by choosing suitable mix solvents and using high-leg-numbered template molecules as porogens. GISAXS is a powerful tool for evaluating pore structural parameters including shape, size, size distribution, electron density, and porosity. The resulting data from GISAXS evaluation show basically agreement with those from optical and electrical measurements. The above results show an effective approach for fabricating nanometer scale porous thin films with ultralow dielectric constant for application in integrated circuits.

Acknowledgment. This work is supported by the Natural Science Foundation of Guangdong Province (No. 0430064), People's Republic of China. Part of this work is based upon research conducted at the CHESS, which is supported by the National Science Foundation and the National Institutes of Health/National Institute of General Medical Sciences under NSF award DMR-0225180, USA.

References and Notes

(1) Kim, T. S.; Mackie, K.; Zhong, Q.; Peterson, M.; Konno, T.; Dauskardt, R. H. *Nano Lett.* **2009**, *9*, 2427.
(2) Jiang, Y. B.; Xomeritakis, G.; Chen, Z.; Dunphy, D.; Kissel, D. J.; Cecchi, J. L.; Brinker, C. J. *J. Am. Chem. Soc.* **2007**, *129*, 15446.
(3) Gin, D. L.; Gu, W. *Adv. Mater.* **2001**, *13*, 1407.
(4) Yant, Y.; Bein, T. *J. Am. Chem. Soc.* **1995**, *117*, 9990.
(5) Radu, D, R.; Lai, C.-Y; Wiench, J. W.; Pruski, M.; Lin, V. S.-Y *J. Am. Chem. Soc.* **2004**, *126*, 1640.
(6) Li, Y. Y.; Cunin, F.; Link, J. R.; Gao, T.; Betts, R. E.; Reiver, S. H.; Chin, V.; Bhatia, S. N.; Sailor, M. J. *Science* **2003**, *299*, 2045.
(7) Miller, R. D. *Science* **1999**, *286*, 421.
(8) Cha, B. J.; Kim, S.; Char, K.; Lee, J.-K.; Yoon, D, Y.; Rhee, H.-W. *Chem. Mater.* **2006**, *18*, 378.
(9) Su, R. Q.; Muller, T. E.; Prochazka, J.; Lercher, J. A. *Adv. Mater.* **2002**, *14*, 1369.
(10) Ro, H. W.; Kim, K. J.; Theato, P.; Gidley, D. W.; Yoon, D. Y. *Macromolecules* **2005**, *38*, 1031.
(11) Falcaro, P.; Costacurta, S.; Mattei, G.; Amenitsch, H.; Marcelli, A.; Guidi, M. C.; Piccinini, M.; Nucara, A.; Malfatti, L.; Kidchob, T.; Innocenzi, P. *J. Am. Chem. Soc.* **2005**, *127*, 3838.
(12) Walheim, S.; Schäffer, E.; Mlynek, J.; Steiner, U. *Science* **1999**, *283*, 520.
(13) Lei, C.; Shin, Y.; Liu, J.; Ackerman, E. J. *J. Am. Chem. Soc.* **2002**, *124*, 11242.
(14) Eslava, S.; Iacopi, F.; Baklanov, M. R.; Kirschhock, C. E. A.; Maex, K.; Martens, J. A. *J. Am. Chem. Soc.* **2007**, *129*, 9288.
(15) Kuang, D.; Brezesinski, T.; Smarsly, B. *J. Am. Chem. Soc.* **2004**, *126*, 10534.
(16) Yang, Y.; Lu, Y.; Lu, M.; Huang, J.; Haddad, R.; Xomeritakis, G.; Liu, N.; Malanoski, A. P.; Sturmayr, D.; Fan, H.; Sasaki, D. Y.; Assink, R. A.; Shelnutt, J. A.; Swol, F.; Lopez, G. P.; Burns, A. R.; Brinker, C. J. *J. Am. Chem. Soc.* **2003**, *125*, 1269.
(17) Shimojima, A.; Liu, Z.; Ohsuna, T.; Terasaki, O.; Kuroda, K. *J. Am. Chem. Soc.* **2005**, *127*, 14108.
(18) Tang, J.; Zhou, X.; Zhao, D.; Lu, G. Q.; Zou, J.; Yu, C. *J. Am. Chem. Soc.* **2007**, *129*, 9044.
(19) Zhou, Y.; Schattka, J. H.; Antonietti, M. *Nano Lett.* **2004**, *4*, 477.
(20) Freer, E. M.; Krupp, L. E.; Hinsberg, W. D.; Rice, P. M.; Hedrick, J. L.; Cha, J. N.; Miller, R. D.; Kim, H.-C. *Nano Lett.* **2005**, *5*, 2014.
(21) Pai, R. A.; Humayun, R.; Schulberg, M. T.; Sengupta, A.; Sun, J.-N.; Watkins, J. J. *Science* **2004**, *303*, 507.
(22) Tanaka, S.; Nishiyama, N.; Oku, Y.; Egashira, Y.; Ueyama, K. *J. Am. Chem. Soc.* **2004**, *126*, 4854.
(23) Lee, B.; Park, Y.-H.; Hwang, Y.-T.; Oh, W.; Yoon, J.; Ree, M. *Nat. Mater.* **2005**, *4*, 147.
(24) Lee, B.; Oh, W.; Hwang, Y.; Park, Y.-H.; Yoon, J.; Jin, K.-S.; Heo, K.; Kim, J.; Kim, K.-W.; Ree, M. *Adv. Mater.* **2005**, *17*, 696.
(25) Kim, H.-C.; Wallraff, G.; Kreller, C. R.; Angelos, S.; Lee, V. Y.; Volksen, W.; Miller, R. D. *Nano Lett.* **2004**, *4*, 1169.
(26) Tanaka, S.; Tate, M. P.; Nishiyama, N.; Ueyama, K.; Hillhouse, H. W. *Chem. Mater.* **2006**, *18*, 5461.
(27) Chen, H.-J.; Fu, M. *Macromolecules* **2007**, *40*, 2079.
(28) Kim, H.-C.; Kreller, C. R.; Tran, K. A.; Sisodiya, V.; Angelos, S.; Wallraff, G.; Swansom, S.; Miller, R. D. *Chem Mater.* **2004**, *16*, 4267.
(29) Zhao, G.; Ishizaka, T.; Kasai, H.; Hasegawa, M.; Furukawa, T.; Nakanishi, H.; Oikawa, H. *Chem. Mater.* **2009**, *21*, 419.
(30) Oh, W.; Hwang, Y.; Park, Y. H.; Ree, M.; Chu, S.-H.; Char, K.; Lee, J. K.; Kim, S. Y. *Polymer* **2003**, *44*, 2519.
(31) Pang, J.; Xiong, S.; Jaeckel, F.; Sun, Z.; Dunphy, D.; Brinker, C. J. *J. Am. Chem. Soc.* **2008**, *130*, 3284.
(32) Verploegen, E.; Zhang, T.; Jung, Y. S.; Ross, C.; Hammond, P. T. *Nano Lett.* **2008**, *8*, 3434.
(33) Small-angle X-ray scattering (SAXS) measurements for the porogens were performed in solutions of methyl isobutyl ketone (MIBK) and conducted at the Beamlines of the Synchrotron Radiation Laboratory, Institute of High Energy Physics, Chinese Academy of Sciences, Beijing, an X-ray radiation source with $\lambda = 0.154$ nm and a two-dimensional charge-coupled device (2D CCD) detector with a sample-to-detector distance of 5230 mm. Optical experimental measurements of refractive indices and thin film thicknesses were performed on a spectroscopic ellipsometer (model TP-71, Beijing, China) equipped with a hot stage and a Xe lamp light source. The refractive index properties of all thin films were investigated by spectroscopic ellipsometry using the previously reported method at 632.6 nm wavelengths, and corresponding dielectric constants (ε_∞) of them were estimated according to the well-known Maxwell−Garnett equation. Dielectric constants (ε) were measured at 1 MHz using an Agilent impedance analyzer (model HP4294A). All GISAXS measurements were conducted at the D1 beamline of the Cornell High Energy Synchrotron Source (CHESS), Cornell University. The sample-to-detector distance was 937 mm for an X-ray radiation source with a wavelength of $\lambda = 0.123$ nm, and a two-dimensional charge-coupled device (2D CCD) detector was used.
(34) Frömsdorf, A.; Capek, R.; Roth, S. V. *J. Phys. Chem. B* **2006**, *110*, 15166.
(35) Leroy, F.; Lazzari, R.; Renaud, G. *Acta. Crystallogr., Sect. A* **2004**, *60*, 565.
(36) Lazzari, R.; Leroy, F.; Renaud, G. *Phys. Rev. B* **2007**, *76*, 125411.
(37) Rauscher, M.; Salditt, T.; Spohn, H. *Phys. Rev. B* **1995**, *52*, 16855.
(38) Holy, V.; Pietsch, U.; Baumbach, T. *High-resolution X-ray scattering from thin films and multilayers*; Springer: Berlin, 1999).
(39) Parratt, L. G. *Phys. Rev.* **1954**, *95*, 359.
(40) Pedersen, J. S. *J. Appl. Crystallogr.* **1994**, *27*, 595.
(41) Valiskó, M.; Boda, D. *J. Phys. Chem. B* **2005**, *109*, 6355.
(42) Kim, C.-S.; Jeong, H.-D. *J. Phys. Chem. B* **2008**, *112*, 16257.

JP905457B